ELSEVIER

Biophysical Chemistry 94 (2001) 23–31

Biophysical Chemistry

www.elsevier.com/locate/bpc

Thermodynamic and computational studies of DNA triple helices containing a nucleotide or a non-nucleotide linker in the third strand

Concetta Giancola*, Luigi Petraccone, Maria Pieri, Guido Barone

Department of Chemistry, University 'Federico II' of Naples, Via Cintia, Monte Sant' Angelo, 80126 Naples, Italy

Received 4 June 2001; received in revised form 31 July 2001; accepted 3 August 2001

Abstract

In this paper we report a thermodynamic characterisation of stability and melting behaviour of four different triple helices at pH 6.0. The target duplex consists of 16 base pairs in alternate sequence of the type 5′-(purine)$_m$(pyrimidine)$_m$-3′. The four triplexes are formed by targeting the 16-mer duplex with an all pyrimidine 16-mer or 15-mer or 14-mer third strand. The 16-mer oligonucleotide contains a 3′-3′ phosphodiester junction and corresponding triplex was named 16-mer P. The 14-mer oligonucleotide contains a non-nucleotide linker, the 1,2,3 propanetriol residue and the corresponding triplex was named 14-mer PT. For the 15-mer oligonucleotide both junctions were alternatively used and the relative triplexes were named 15-mer P and 15-mer PT, respectively. These linkers introduce the appropriate polarity inversion and let the third strand switch from one oligopurine strand of the duplex to the other. Thermal denaturation profiles indicate the initial loss of the third strand followed by the dissociation of the target duplex. Transition enthalpies, entropies and free energies were derived from differential scanning calorimetric measurements. The comparison of Gibbs energies reveals that a more stable triplex is obtained when in the third strand there is the lack of one nucleotide in the junction region and a propanetriol residue as linker was used. The thermodynamic data were discussed in light of molecular mechanics and dynamics calculations.

Keywords: DNA triple helix; Thermodynamic stability; Differential scanning calorimetry; Computer simulation

* Corresponding author. Tel.: +39-081-674266; fax: +39-081-674090.
E-mail address: giancola@chemistry.unina.it (C. Giancola).

0301-4622/01/$ - see front matter
PII: S0301-4622(01)00205-8

1. Introduction

Oligonucleotide-directed triple helix formation is a unique way to design specific ligands that recognise double-stranded DNA. The interest in the triple helices arises first of all from the possibility of using them to modulate biological processes within a living organism at several levels, such as the transcription which many in vitro and in vivo experiments have recently demonstrated [1–3].

Oligonucleotides of defined sequence can bind to the major groove of double-stranded DNA to form triple helices by recognition of the oligopurine-rich strand. This recognition process is extremely simple, specific and efficient. Specificity derives from tymine (T) recognition of the adenine-tymine Watson–Crick base pair (A·T) and protonated cytosine (C^+) recognition of the guanine–cytosine Watson–Crick base-pair (G·C). The corresponding triplets are indicated as (T × A·T) and (C^+ × G·C), where the symbol · indicates the hydrogen bonds of the Watson and Crick duplex and the symbol × the hydrogen bonds of the triplex. These bonds are indicated as Hoogsteen-bonds, if the third strand orientation is parallel to the double helix purine-rich strand, or reverse-Hoogsteen, if the third strand orientation is anti-parallel to the double helix purine-rich strand. The formation of the (C^+ × G·C) triad requires the protonation of the N3 of the cytosine in the third strand. The efficiency of the single strand binding depends on several factors, such as pH, cation concentration, composition and length of the third strand.

The so-called 'antigene strategy' is based on highly specific recognition of DNA by the third oligonucleotide strand. In order to realise a selective recognition of the DNA target sequence, the third strand must be relatively long, 15–16 bases, but such long homopurine–homopyrimidine stretches are infrequent. In order to increase the number of potential targets for triplex formation in natural DNAs, many research groups have designed alternate strand triplexes [4–6]. In this class of triplexes, the third strand is composed of two adjacent and alternating oligopurine–oligopyrimidine tracts, and presents a junction which assures the opportune inversion of polarity, a 3′–3′ or a 5′–5′ junction, so that the third strand retains the correct orientation respect to the DNA double helix. The third strand crosses the DNA major groove, switching from one oligopurine strand to another at the junction [7,8]. The use of a suitable linker is therefore required to join the 3′–3′ or 5′–5′ ends.

The binding of a third strand to a target double helix generally results in a thermodynamically weaker interaction than observed for the duplex formation itself [9]. The determination of the thermodynamic parameters that govern the relative stability of different classes of triplexes is essential for a comparison of the binding of different oligonucleotides to the same target duplex [10].

The present work is devoted to the comparison of the binding of four 3′–3′ third strands to a 16-mer DNA target duplex, with an alternate purine–pyrimidine sequence. The third strands differ from each other for the number of oligonucleotides, 14-mer, 15-mer or 16-mer, and for the linker that joins the 3′–3′ ends, a 1,2,3-propanetriol residue or a phosphodiester junction. The resulting triplexes are shown in Fig. 1. These triplexes consist of an alternating sequence of (T × A·T) and (C^+ × G·C) triads. Previous studies suggested that blocks of (C^+ × G·C) triplets are unstable, because of the repulsion between adjacent positive charge [11], the stacking energies decrease in the order TAT/CGC^+, TAT/TAT and CGC^+/CGC^+ [12]. Consequently the alternate sequences are the most stable. In previous works we showed that these triple helices exhibit intriguing differential properties depending on the number of nucleotides and of the nature of the linker in the third strand [13,14]. To gain further information on observed differential properties, especially in the case of the same sequence and different linkers, we conducted the DSC measurements on 15-mer P and 16-mer P triplex at pH 6.0 and performed an accurate analysis on the thermodynamic parameters of the four triplexes at this pH. Molecular modelling and dynamics were used to predict if and how

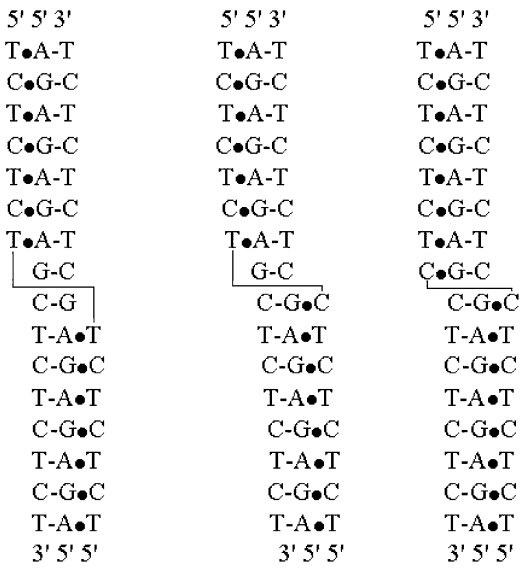

Fig. 1. Schematic representation of the triple helices formed by targeting the 16-mer duplex with a 14-mer, 15-mer or 16-mer third strand. The 14-mer PT triplex (on the left) contains the 1,2,3-propanetriol residue in the third strand. The 16-mer P triplex (on the right) contains a 3′–3′ phosphodiester bond in the third strand. In the 15-mer triplex (in the middle) the third strand contains the 1,2,3-propanetriol residue (15-mer PT) or the phosphodiester bond (15-mer P).

such structures might be formed in an energetically flexible manner. The thermodynamic data are discussed in relation to structural models.

2. Experimental

2.1. Oligonucleotides

The oligonucleotides were synthesised by standard automated solid-support chemistry on a Millipore Cyclone Plus DNA using a phosphoramidite procedure [11]. The third strands containing the junction have been conveniently synthesised through a solid phase procedure involving only 3′-phosphoramidite nucleosides, and starting from a modified support that links the first nucleotide through the base [12]. Deprotected oligonucleotides were purified by HPLC anion-exchange chromatography, using a Nucleogen column [15]. Duplex and triplex samples were prepared in phosphate buffer (5 mM) containing KCl (140 mM) and $MgCl_2$ (5 mM). The concentration of oligonucleotide solution was determined spectrophotometrically using the extinction coefficients at 260 nm calculated by a nearest neighbour model [16]. The triplexes were formed by mixing stoichiometric amounts of the oligonucleotides and then heating to 90°C for 5 min, followed by slow cooling to room temperature. The solutions were equilibrated for 1 day at 4°C before performing the experiments.

2.2. Differential scanning calorimetry

DSC measurements were performed using a DSC II Microcalorimeter from Setaram. The DSC was equipped with a matched pair of 0.8-ml sample and reference cells. In the DSC scans, both cells were first loaded with buffer solution, equilibrated at 0°C for 30 min, and scanned from 0 to 90°C at scan rate of 0.5°C min^{-1}. The sample vs. buffer scan was performed using the same procedure.

The instrument was interfaced with an IBM PC computer for automatic data collection and analysis using the software previously described [17]. The apparent molar heat capacity vs. temperature profiles were obtained by subtracting buffer vs. buffer curves from the sample vs. buffer curves. The data were normalised with regard to the concentration, sample volume and scan rate. The excess heat capacity function $\langle \Delta C_P \rangle$ was obtained after baseline subtraction, assuming that the baseline is given by the linear temperature dependence of the native state heat capacity [18].

The reversibility of the thermal processes was verified by checking the reproducibility of the calorimetric trace in a second heating of the samples immediately after cooling from the first scan.

The process enthalpies for the double helix alone, $\Delta H°(T_m)$, were obtained by integrating the area under the heat capacity vs. temperature curves. T_m is the temperature corresponding to the maximum of each DSC peak. The entropy changes for the double helix alone, $\Delta S°(T_m)$, were determined by integrating the curve obtained by

dividing the heat capacity curve by the absolute temperature. van't Hoff values were obtained by DSC profiles utilising the equation:

$$\Delta H_{vH}^{\cdot} = 6RT_m^2 \Delta C_p^{\cdot}(T_m)/\Delta H^{\cdot}\ (T_m) \quad (1)$$

where T_m is the maximum of DSC peak, $\Delta C_p^{\circ}(T_m)$ is the value of the excess heat capacity function at T_m and $\Delta H^{\cdot}(T_m)$ is the calorimetric enthalpy directly obtained by the area under DSC peak.

The calorimetric melting profiles of the triple helices, composed of two palindromic strands and one third strand, were modelled by two sequential bimolecular transitions:

$$A_2B \overset{K_1}{\leftrightarrow} A_2 + B \overset{K_2}{\leftrightarrow} 2A + B$$

where A_2B indicates the triple helix, A_2 the target duplex, A each palindromic duplex strand and B the third strand.

Considering the stoichiometry and conservation of mass the following equations hold at any temperature:

$$C_t = C_{A_2B} + C_{A_2} + 1/2C_A \quad (2)$$

$$C_t = C_{A_2B} + C_B \quad (3)$$

$$C_{A_2} + 1/2C_A = C_B \quad (4)$$

where C_t is the molar concentration of the third strand, it corresponds to the concentration of the double helix and, at low temperature, of triple helix too.

The fractional population of each species can be defined as:

$$f_x = \frac{C_x}{C_t} \quad (5)$$

where x represent A_2B, A_2 and B and the above equations can be rewritten as:

$$f_{A_2B} + f_{A_2} + 1/2\ f_A = 1 \quad (6)$$

$$f_{A_2B} + f_B = 1 \quad (7)$$

$$f_{A_2} + 1/2\ f_A = f_B \quad (8)$$

The two equilibrium constants, K_1 and K_2, are:

$$K_1 = \frac{f_{A_2} f_B}{f_{A_2B}} C_t \quad (9)$$

$$K_2 = \frac{f_A^2}{f_{A_2}} C_t \quad (10)$$

Combining the above relations the following coupled non-linear equations result:

$$f_B = \frac{1 - f_B}{f_{A_2}} \frac{K_1}{C_t} \quad (11)$$

$$f_{A_2} = 4(f_B - f_{A_2})^2 \frac{C_t}{K_2} \quad (12)$$

The resolutions of the set of the Eqs. (11) and (12) can be introduced in the equation of the excess enthalpy:

$$\langle \Delta H \rangle = f_B \Delta H_1 + (f_B - f_{A_2}) \Delta H_2 \quad (13)$$

where f_{A_2} and f_B are the fractional populations of duplex and single strand and ΔH_1 and ΔH_2 are the enthalpy changes of the two sequential transitions.Then the excess heat capacity, $\langle \Delta C_p \rangle$, can be calculated:

$$\langle \Delta C_p \rangle = \frac{\partial \langle \Delta H \rangle}{\partial T} \quad (14)$$

At any temperature the equilibrium constants have be determined according to the equation:

$$K_i = K_i(T_{mi}) e^{(-\frac{\Delta H_i}{R})(\frac{1}{T} - \frac{1}{T_{mi}})} \quad (15)$$

where we assumed that the T_m are the temperatures at which K_i are equal to $C_t/2$.

Eqs. (11) and (12) were solved numerically for the fractional populations and the heat capacity

subsequently determined through numerical differentiation of Eq. (13), using a self-made MATHLAB program and assuming that the ΔH_i values were constant. T_m and ΔH_i values reported in Table 1 provide the best fit of the experimental triplex denaturation curves. The global simulated excess heat capacity curves were split in the two corresponding subtransitions defined by:

$$\langle \Delta C_{p,i} \rangle = \Delta H_i \frac{\partial f_i}{\partial T} \quad (16)$$

where f_i is f_B or $f_B - f_{A_2}$ [Eq. (13)].

The ΔS_i° values were calculated integrating curves obtained by dividing the two simulated subtransitions curves by the absolute temperatures, i.e. $\Delta S_i^\circ = \int(\langle \Delta C_{p,i} \rangle / T)\mathrm{d}T$.

2.3. Molecular mechanics and dynamics

The 15-mer PT and the 15-mer P triplexes have been studied using molecular mechanics (MM) and molecular dynamics (MD).

Models of the two triplexes were built from the helical coordinates given by Liu [19]. The two 3′-ends at the junction site of the third strand were linked by a phosphate group or by a 1,2,3 propanetriol residue for the 15-mer P and 15-mer PT, respectively. The charges on the atoms of protonated cytosines were modified in order to take the protonation into account.

The two triplexes were neutralised by adding sodium counterions and then, each triplex was individually placed in a 30.1 Å × 30.1 Å × 56.1 Å box of Monte Carlo TIP3P water, with periodic boundary conditions. Water molecules closer than 2.3 Å from the solute atoms were removed. For both triplexes the same energy minimisation and dynamics procedure were used.

The Amber force field [20] was utilised and a cut-off of 12 Å was applied to the non-bonded potential. Starting structures were minimised using 1500 steps of the steepest descent method followed by the conjugate method until convergence to a r.m.s. gradient of 0.1 kcal mol^{-1} Å^{-1}.

MD runs were started by assigning random velocities, that followed a Gaussian distribution at 10 K. The systems were heated from 10 to 300 K by coupling to a heating bath over a period of 6 ps. Then for both the triplexes constant temperature dynamics were performed over a period of 94 ps without any restraints, resulting in a 100-ps MD realisation. A 0.5-fs integration time step was used. After a 14 ps of equilibration at 300 K snapshots were collected every 0.1 ps for 80 ps.

3. Results and discussion

The calorimetric curves of the 15-mer P and 16-mer P triplexes and the target duplex are shown in Fig. 2. The thermal denaturation of the

Table 1
Comparison of the thermodynamic parameters for the transition processes of the four triplexes and the target duplex at pH 6.0

	T_m [a] (°C)	$\Delta H°(T_m)$ (kJ mol^{-1})	$\Delta S°(T_m)$ (kJ mol^{-1} K^{-1})	$\Delta G°(T_m)$ (298) (kJ mol^{-1})
16-mer P	45.9	260 ± 8	0.816 ± 0.04	16.8
	69.0	425 ± 15	1.250 ± 0.06	79.3
15-mer P	41.0	260 ± 11	0.743 ± 0.03	38.6
	69.1	400 ± 22	1.180 ± 0.03	78.2
15-mer PT	44.0	255 ± 10	0.705 ± 0.02	44.9
	69.1	418 ± 13	1.220 ± 0.07	78.3
14-mer PT	39.0	265 ± 8	0.850 ± 0.02	11.7
	69.1	427 ± 23	1.260 ± 0.06	81.3
Duplex	69.2	430 ± 18	1.170 ± 0.04	81.3

[a] The error in T_m does not exceed 0.2°C. Thermodynamic data for each triplex are relative to dissociation processes: $A_2B \Leftrightarrow A_2 + B$ (first line) and $A_2 \Leftrightarrow 2A$ (second line).

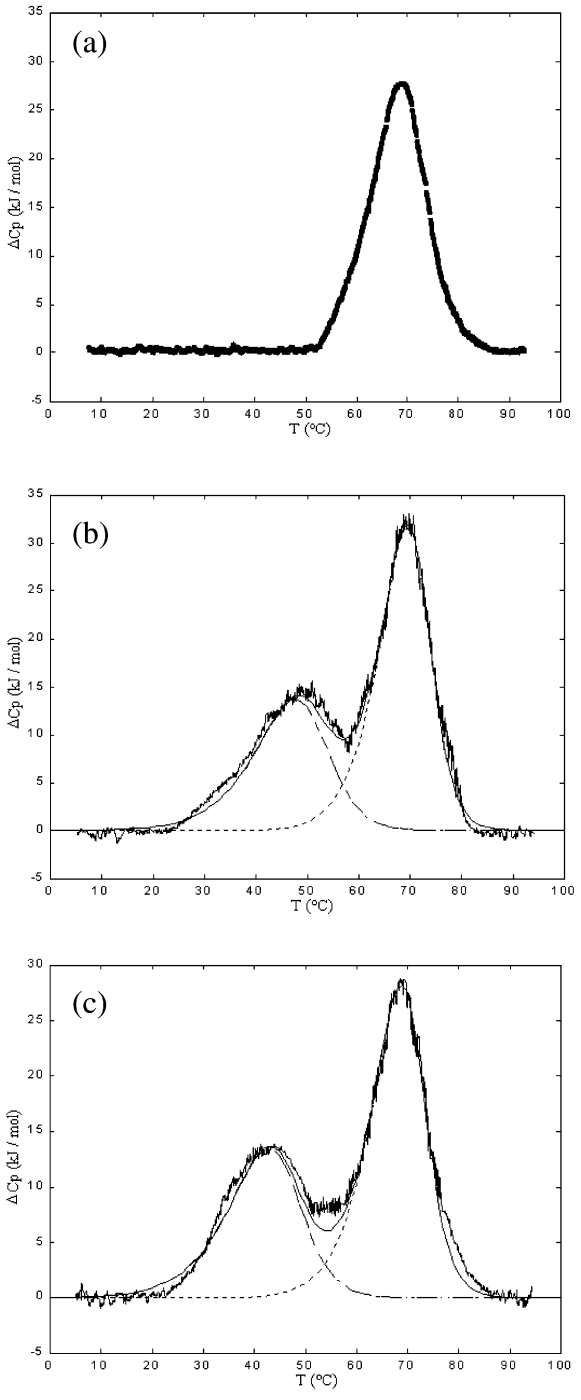

Fig. 2. Excess heat capacity of the target duplex (panel A), 15-mer P triplex (panel B) and 16-mer P triplex (panel C): experimental data (bold line), total simulated transition (solid line) and deconvolution in two transitions (dash dotted line and dashed line). The concentrations were 72 μM.

duplex and all the triplexes is completely reversible. This is important because the reversibility is necessary in determining $\Delta G°$ from calorimetric data and in estimating the model-dependent thermodynamic parameters using van't Hoff analysis. Inspection of the calorimetric transition profiles reveals that all the curves are biphasic, with the low-temperature transition due to the dissociation of the third strand from the target duplex and the high temperature transition, centred at 69.0°C, due to the dissociation of the double helix into two strands. As the two transitions are not well separated a deconvolution procedure was used (see Section 2).

The good agreement between the calculated and the experimental curves induced us to apply the deconvolution procedure to the thermal denaturation profiles of the 14-mer PT and the 15-mer PT triplexes previously reported [14]. The data are collected in Table 1.

The enthalpy of duplex strand dissociation is essentially identical in the presence and absence of the third strand. These values are in satisfactory agreement with the predicted enthalpy change of 444 kJ mol^{-1} calculated from nearest neighbour analysis, according to the method of Santalucia [21]. The values of ΔH°_{vH} obtained for the first dissociation are consistent with a two-state transition model and are close to 18–24 kJ mol^{-1} bt^{-1} estimated by Asensio et al. [22].

The Gibbs energy values were calculated at 298 K using the standard thermodynamic relationship $\Delta G^{\circ} = \Delta H^{\circ} - T\Delta S^{\circ}$ and assuming a negligible difference in heat capacity between the initial and final states. The calorimetric profiles do not show significant ΔC_p for all the studied triplexes, as already found in DSC studies on triple helices [8,23,24].

Inspection of thermodynamic data of the two triplexes containing the 1,2,3 propanetriol linker reveals that the 15-mer PT is thermally more stable than 14-mer PT, ΔT being 5.0°C. The two triplexes differ in the presence of the cytidine monophosphate in the junction region of the third strand. The target duplex contains one base pair (15-mer PT) or two base pairs (14-mer PT) that do not participate in Hoogsteen H-bonds, these bases are spanned by the linker. In term of the

Gibbs energy change the lack of a cytidine monophosphate in the junction region decreases the stability by 33.2 kJ mol^{-1} (44.9 kJ mol^{-1} vs. 11.7 kJ mol^{-1}). Since the $\Delta H^{\circ}(T_m)$ values are equal and the T_m of the 15-mer PT is greater than that of 14-mer PT, the major thermodynamic stability of 15-mer PT is entropically controlled. In fact, the entropy change of 15-mer PT formation is less unfavourable than that of 14-mer PT.

In the case of the triplexes containing the phosphodiester bond, the ΔG° values, at 298 K, of 15-mer P and 16-mer P are 38.6 and 16.8 kJ mol^{-1}, respectively. This trend in the free energy term is not reflected by the T_m values demonstrating that the cytidine monophosphate in the junction region is entropically unfavourable.

It is interesting to compare the two triple helices (15-mer P and 15-mer PT) containing the same number of nucleotides in the third strands but a different 3′–3′ junction. The T_m of the 15-mer PT is higher than the T_m of the 15-mer P (44°C vs. 41°C). The calculated ΔG° values at 298 K are 44.9 and 38.6 kJ mol^{-1}, respectively. Although the 15-mer PT has a higher free energy, the triplex containing the 1,2,3 propanetriol residue is more stable by 6.3 kJ mol^{-1}. In order to visualise the geometry of the triplexes corresponding to the two 3′–3′ junctions we performed the molecular mechanics calculations in the presence of explicit water and counterions. The obtained structures are very similar and all the bases of the third strands form the Hoogsteen H-bonds after minimisation (Fig. 3). The structures of the duplex in the free and triplex state are similar suggesting that the duplex is predisposed to accepting the third strand into its major groove and only minor readjustments of the duplex are needed to form these triplexes.

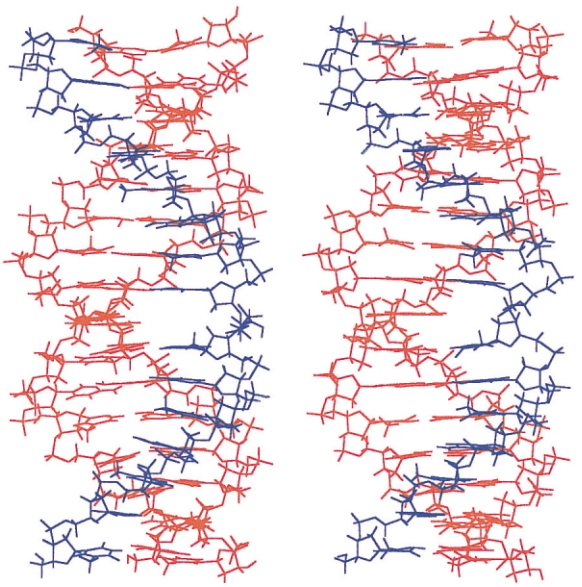

Fig. 3. Triple helical structures of the 15-mer PT triplex (on the left) and 15-mer P triplex (on the right) generated by molecular mechanics. The Watson–Crick strands are shown in red and the third strands are shown in blue.

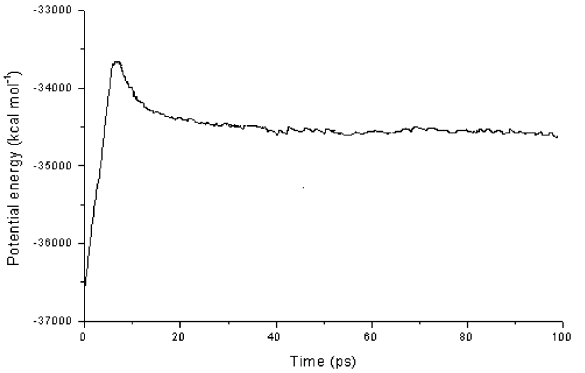

Fig. 4. Plot of potential energy for the MD simulation of 15-mer PT triplex over the heating (0–6 ps), equilibration (6–20 ps) and data collection (20–100 ps) phases. A similar plot was obtained for the 15-mer P trajectory.

To better characterise the structural stability of the two triplexes and to investigate whether the H-bond scheme of the two triplexes shows some difference, particularly in the junction region, the two structures were subjected to a constant temperature MD simulation at 300 K, in the presence of explicit water and counterions. From the plot of potential energy against time (Fig. 4) it was clear that, after an equilibration phase involving the first 20 ps, the system became energetically stable for the last 80 ps of the simulation. The integrity of the two triple helices is maintained throughout all the simulations, even though no constraints are introduced to reinforce the H-

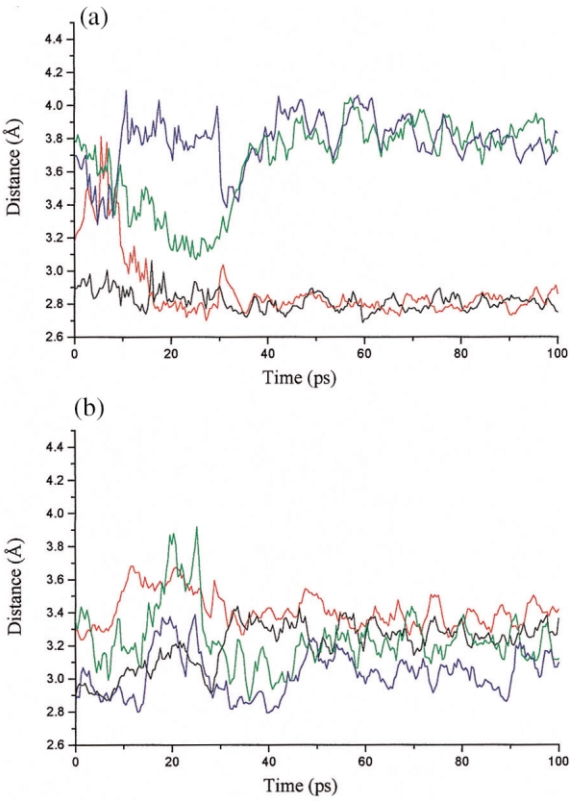

Fig. 5. Hoogsteen hydrogen bond distances during the MD trajectory for the T and C bases involved in the junction of the 15-mer PT triplex (panel A) and the 15-mer P triplex (panel B). For both the triplexes the N7(A)-N3(T) H-bond is shown in blue, the N6(A)-O4(T) H-bond is shown in green, N7(G)-N3(C) is shown in red and O6(G)-N4(C) is shown in black.

bonds. Some differences in molecular dynamics studies were observed for the two central triplets of the two macromolecules. Fig. 5 shows the Hoogsteen H-bond distance of these central triplets during the MD simulation. Analysis of the H-bonds formed by the two bases involved in the junctions (T, C), demonstrated that the Hoogsteen H-bonds for the 15-mer P triplex are maintained during almost the entire trajectory (Fig. 5, panel B). In the 15-mer PT the N7(A)-N3(T) H-bond is lost during almost the entire trajectory, while the N6(A)-O4(T) H-bond is observed during ~17% of the trajectory, when the N–O distance is minor than 3.5 Å (Fig. 5, panel A). These findings reflect a certain degree of flexibility of the propanetriol-linker with respect to the phosphate-linker. Hence, MD simulations suggest that the 15-mer P triplex possesses a more rigid structure with a lower entropy. This could justify the major entropic gain for the dissociation process of 15-mer P triplex and consequently the 15-mer PT triplex results are more stable.

In conclusion, the 1,2,3 propanetriol residue has proved to be an efficient and flexible non-nucleotide linker for 3′–3′ oligonucleotides to be used as triple helix forming oligonucleotides in an alternate strand recognition approach. The stability is enhanced when the linker spans one base pair rather than two base pairs of the target duplex.

Acknowledgements

This work was supported by a PRIN-MURST grant from the Italian Ministry and University and Scientific and Technological Research (Rome).

References

[1] D. Praseuth, A.L. Guieysse, C. Hélène, Triple helix formation and the antigene strategy for sequence-specific control of gene expression, Biochim. Biophys. Acta 1489 (1999) 181–206.

[2] M. Faria, C.D. Wood, L. Perrouault et al., Targeted inhibition of transcription elongation in cells mediated by triplex-forming oligonucleotides, Proc. Natl. Acad. Sci. USA 97 (2000) 3862–3867.

[3] F.X. Barre, S. Ait-Si-ali, C. Giovannangeli, R. Luis et al., Unambiguous demonstration of triple-helix-directed gene modification, Proc. Natl. Acad. Sci. USA 97 (2000) 3084–3088.

[4] A. Ono, C.N. Chen, L. Kan, DNA triplex formation of oligonucleotide analogues consisting of linker groups and octamer segments that have opposite sugar-phosphate backbone polarities, Biochemistry 30 (1991) 9914–9921.

[5] B.C. Froehler, T. Terhorst, J.-P. Shaw, S.N. McCurdy, Triple-helix formation and cooperative binding by oligodeoxynucleotides with a 3′–3′ internucleotide junction, Biochemistry 31 (1992) 1603–1609.

[6] B.W. Zhou, C. Marchand, U. Asseline et al., Recognition of alternating oligopurine/oligopyrimidine tracts of DNA by oligonucleotides with base-to-base linkages, Bioconjugate Chem. 6 (1995) 516–523.

[7] D.A. Horne, P.B. Dervan, Recognition of mixed-sequence duplex DNA by alternate-strand triple-helix formation, J. Am. Chem. Soc. 112 (1990) 2435–2437.
[8] C. Giancola, A. Buono, G. Barone et al., Thermodynamics of a 24-mer triple helix formation and stability, J. Thermal Anal. Cal. 56 (1999) 1177–1184.
[9] R.H. Shafer, in: K. Moldave (Ed.), Progress in Nucleic Acid Research, Academic Press Inc, San Diego, CA.
[10] M. Mills, P.B. Arimondo, L. Lacroix et al., Energetics of strand-displacement reactions in triple helices: a spectroscopic study, J. Mol. Biol. 291 (1999) 1035–1054.
[11] L.L. Kiessling, L.C. Griffin, P.B. Dervan, Flanking sequence effects within the pyrimidine triple-helix motif characterized by affinity cleaving, Biochemistry 31 (1992) 2829–2834.
[12] J. Chomilier, J.-S. Sun, D.A. Collier, T. Garestier, C. Hélène, R. Lavery, A computational and experimental study of the bending induced at a double-triple helix junction, Biophys. Chem. 45 (1992) 143–145.
[13] C. Giancola, M. Pieri, L. Petraccone, D. Montesarchio, G. Barone, Thermodynamic and conformational properties of DNA triplexes containing 3′–3′ phosphodiester bond, Thermochim. Acta 372 (2001) 129–136.
[14] C. Giancola, L. Petraccone, M. Pieri et al., Physicochemical studies on DNA triplexes containing an alternate third strand with a non-nucleotide linker, Int. J. Biol. Macromol. 28 (2001) 387–394.
[15] T. Brown, D.J.S. Brown, Purification of synthetic DNA, Methods Enzymol. 211 (1992) 20–35.
[16] C.R. Cantor, M.M. Warshaw, H. Shapiro, Oligonucleotide interactions. Circular dichroism studies of the conformation of deoxyoligonucleotides, Biopolymers 9 (1970) 1059–1077.
[17] G. Barone, P. Del Vecchio, D. Fessas, C. Giancola, G. Graziano, Theseus: a new software package for the handling and analysis of thermal denaturation data of biological macromolecules, J. Thermal Anal. 39 (1993) 2779–2790.
[18] E. Freire, R.L. Biltonen, Thermodynamics of transfer ribonucleic acids: the effect of sodium on the thermal unfolding of yeast tRNAPhe, Biopolymers 17 (1978) 1257–1272.
[19] K. Liu, V. Sasisekharan, H.T. Miles, Structure of Py·Pu·Py DNA triple helices. Fourier transforms of fiber-type X-ray diffraction of single crystals, Biopolymers 39 (1996) 573–589.
[20] W.D. Cornell, P. Cieplak, C.I. Bayly et al., A second generation force field for the simulation of proteins, nucleic acids and organic molecules, J. Am. Chem. Soc. 117 (1995) 5179–5197.
[21] J. Santalucia, H.T. Allawi, P.A. Seneviratne, Improved nearest-neighbor parameters for predicting DNA duplex stability, Biochemistry 35 (1996) 3555–3562.
[22] J.L. Asensio, A.N. Lane, J. Dhesi, S. Bergqvist, T. Brown, The contribution of cytosine protonation to the stability of parallel DNA triple helices, J. Mol. Biol. 275 (1998) 811–822.
[23] G.E. Plum, K.J. Breslauer, Thermodynamics of an intramolecular DNA triple helix: a calorimetric and spectroscopic study of the pH and salt dependence of thermally induced structural transitions, J. Mol. Biol. 248 (1995) 679–695.
[24] H.P. Hopkins, D.D. Hamilton, W.D. Wilson, G. Zon, Duplex and triple helix formation with dA19 and dT19. Thermodynamic parameters from calorimetric, NMR, and circular dichroism studies, J. Phys. Chem. 97 (1993) 6555–6563.